

# The v-ATPase V<sub>0</sub> Subunit a1 Is Required for a Late Step in Synaptic Vesicle Exocytosis in *Drosophila*

P. Robin Hiesinger,<sup>1</sup> Amir Fayyazuddin,<sup>2</sup>  
Sunil Q. Mehta,<sup>3</sup> Tanja Rosenmund,<sup>2</sup>  
Karen L. Schulze,<sup>1</sup> R. Grace Zhai,<sup>1</sup>  
Patrik Verstreken,<sup>2</sup> Yu Cao,<sup>2</sup> Yi Zhou,<sup>2</sup>  
Jeannette Kunz,<sup>4</sup> and Hugo J. Bellen<sup>1,2,3,5,\*</sup>

<sup>1</sup>Howard Hughes Medical Institute

<sup>2</sup>Department of Molecular and Human Genetics

<sup>3</sup>Program in Developmental Biology

<sup>4</sup>Department of Molecular Physiology and Biophysics

<sup>5</sup>Department of Neuroscience

Baylor College of Medicine

Houston, Texas 77030

## Summary

The V<sub>0</sub> complex forms the proteolipid pore of an ATPase that acidifies vesicles. In addition, an independent function in membrane fusion has been proposed largely based on yeast vacuolar fusion experiments. We have isolated mutations in the largest V<sub>0</sub> component *vha100-1* in flies in an unbiased genetic screen for synaptic malfunction. The protein is only required in neurons, colocalizes with markers for synaptic vesicles as well as active zones, and interacts with t-SNAREs. Loss of *vha100-1* leads to vesicle accumulation in synaptic terminals, suggesting a deficit in release. The amplitude of spontaneous release events and release with hypertonic stimulation indicate normal levels of neurotransmitter loading, yet mutant embryos display severe defects in evoked synaptic transmission and FM1-43 uptake. Our data suggest that Vha100-1 functions downstream of SNAREs in synaptic vesicle fusion.

## Introduction

Membrane fusion lies at the heart of numerous cell biological processes, most notably vesicle trafficking events underlying cellular function (Jahn, 2004; Jahn et al., 2003; Mayer, 2002). The basic fusion machinery in virtually all membrane fusion assays analyzed to date relies on SNAREs (soluble NSF-attachment protein receptors) (Jahn, 2004; Südhof, 2004). The commonly accepted model for a general membrane fusion machinery denotes that membranes are forced into close proximity by the action of SNAREs. In support of this idea, SNAREs have been shown to be sufficient to drive fusion in numerous assays (Hu et al., 2003; Weber et al., 1998). In contrast to this “proximity model” of membrane fusion, the proteolipid pore-forming V<sub>0</sub> complex has been shown to be required for membrane fusion downstream of SNARE action in a yeast vacuolar fusion assay (Bayer et al., 2003; Peters et al., 2001). Although “pore models” for membrane fusion have been suggested repeatedly in the past, it has been difficult to gather compelling data to verify the presence of a pro-

teolipid pore during membrane fusion (Jahn, 2004; Jena, 2004; Lindau and Almers, 1995; Mayer, 2002; Morel, 2003; Weimer and Jorgensen, 2003).

One of the most intensively studied membrane fusion events is the exocytosis of synaptic vesicles that release neurotransmitter at chemical synapses. Neurotransmitter release is tightly regulated to ensure correct information exchange between neurons and other cells (Südhof, 2004). Consequently, synaptic vesicle fusion is regulated by a complex machinery in which SNARE proteins play a prominent role (Chen and Scheller, 2001; Jahn et al., 2003). Hence, loss of synaptic SNAREs generally causes severe defects in vesicle exocytosis (Deitcher et al., 1998; Jahn, 2004; Richmond and Broadie, 2002; Schulze et al., 1995). The prevalent model states that the SNARE complex stabilizes readily releasable vesicles at the membrane at basal Ca<sup>2+</sup> concentrations. This complex triggers membrane fusion at elevated Ca<sup>2+</sup> levels (Jahn et al., 2003; Sørensen, 2004). Hence, priming for fusion and the actual fusion step are both thought to be directly linked to SNARE function.

The existence of a proteinaceous pore capable of releasing neurotransmitter has first been proposed for vesicles isolated from electroplaques of the electric organ of *Torpedo marmorata*. It was found to consist of the 16 kDa subunit of the v-ATPase V<sub>0</sub> complex and was shown to induce quantal release when expressed in a specific cell line (Falk-Vairant et al., 1996; Israël et al., 1986; Morel, 2003). It should be noted that these studies did not address the role of V<sub>0</sub> proteins at the synapse in vivo and they were met with skepticism, as it is difficult to reconcile that a complex event such as synaptic vesicle exocytosis could be mimicked by transfecting a single protein in cells (Falk-Vairant et al., 1996). More recently, the *Torpedo* V<sub>0</sub> subunit a1 (the ortholog of the fly protein discussed here) was shown to localize specifically to nerve terminals and interact with SNAREs (Morel et al., 2003). However, a direct requirement of V<sub>0</sub> proteolipids for membrane fusion has only been demonstrated for a yeast vacuolar fusion assay (see below; Peters et al., 2001).

The vesicular or vacuolar ATPase is a multisubunit protein complex consisting of a V<sub>1</sub> and V<sub>0</sub> subcomplex (Nelson, 2003; Nishi and Forgac, 2002). The V<sub>1</sub> sector comprises a protein complex that hydrolyzes ATP, providing the energy to pump protons through the proteolipid pore formed by the V<sub>0</sub> sector. The v-ATPases are important proton pumps that acidify a wide variety of intracellular and some extracellular compartments (Nelson, 2003; Nishi and Forgac, 2002). In neurons, loading of synaptic vesicles with neurotransmitter requires the v-ATPase-dependent acidification of synaptic vesicles (Amara and Kuhar, 1993). For the largest V<sub>0</sub> subunit, four genes (*a1–a4*) have been identified in human, mouse, *C. elegans*, and *Drosophila*. In *C. elegans*, the four genes display highly tissue-specific distributions with subunit a1 (*unc-32*) exhibiting predominantly neuronal expression (Oka et al., 2001; Pujol et al., 2001). Similarly, the two subunit a1 proteins in yeast, Vph1p and Stv1p, exhibit strong compartmental specificity,

\*Correspondence: hbellen@bcm.tmc.edu

with Vph1p being the vacuolar version (Kawasaki-Nishi et al., 2001; Perzov et al., 2002). *VPH1*-deficient vacuoles do not fuse in the vacuolar fusion assay (Bayer et al., 2003). The defect was placed downstream of SNARE function and is independent of the decreased acidification of the vacuoles. Hence, *VPH1* provided a means to untangle the role of the v-ATPase  $V_0$  complex in acidification from vacuolar fusion in yeast (Bayer et al., 2003; Peters et al., 2001; Thorngren et al., 2004). However, the relevance of this work for fusion of synaptic vesicles in neurons and other fusion events in yeast has not been documented.

We have isolated mutations in a neuron-specific *VPH1* homolog of the v-ATPase  $V_0$  complex in a forward genetic screen in *Drosophila*. Mutations in *vha100-1* (*v100*), the fly subunit a1, allow a functional analysis of the role of the  $V_0$  complex in neurons. Here, we report that loss-of-function mutations in *vha100-1* indicate a defect late in synaptic vesicle exocytosis. Our data indicate that *Vha100-1* is a regulator of synaptic vesicle fusion efficiency downstream of SNARE-dependent vesicle priming.

## Results

### *vha100-1* (*v100*) Is a Neuronal v-ATPase $V_0$ Subunit a1

In a forward genetic screen for genes involved in synapse formation and function we identified five EMS (ethyl methane sulfonate)-induced alleles of a complementation group named *3R3* (Mehta et al., 2005; Verstreken et al., 2003). We screened mosaic flies in which chromosome arms carrying randomly induced mutations were made homozygous in the visual system using the eyFLP system (Newsome et al., 2000; Stowers and Schwarz, 1999). Flies with eyes homozygous for any of the five alleles of the *3R3* complementation group consistently fail to walk toward light in a phototaxis assay (Figure 1A; Benzer, 1967). Furthermore, all alleles display defects in electroretinograms (ERGs), extracellular recordings that measure the response of photoreceptor neurons to a light stimulus. Group *3R3* eyFLP mutants respond with a normal depolarization to light stimuli, but exhibit a complete loss of “on” and “off” transients, indicative of a failure to evoke a post-synaptic response (Pak et al., 1969; Figure 1B), similar to the ERGs observed in neuronal *synaptobrevin* (*n-syb*) and *synaptotagmin* (*syt*) mutants (Stowers and Schwarz, 1999; data not shown).

We mapped the lethality associated with complementation group *3R3* to a ~50 kb interval at cytological location 98F12 using meiotic recombination mapping with P elements (Figure 1C; Figure 2E in Zhai et al., 2003) and temperature-gradient capillary electrophoresis (Figure 3 in Zhai et al., 2003). As shown in Figure 1D, all five alleles contain single-nucleotide changes: *v100<sup>1</sup>* and *v100<sup>4</sup>* exhibit altered splice acceptor sites predicted to produce short, truncated proteins; *v100<sup>2</sup>* and *v100<sup>3</sup>* cause changes of conserved amino acids in the first transmembrane domain, and *v100<sup>5</sup>* has a premature stop codon (Figures 1D, 1E, and 1G). All mutations fail to complement each other, and all transheterozygous allelic combinations, including any allele

over a deficiency (*Df(3R)3450; 98E3-99A6*) are late embryonic lethal. These data suggest that the five alleles are strong hypomorphic or null alleles. We obtained a cDNA of the *v100* transcript CG1709-RC (shown in green in Figure 1D). Photoreceptor-specific expression of this cDNA rescues the “on” and “off” transients in eyFLP mutants of all alleles, indicating that the ERG phenotypes associated with the eyFLP *v100<sup>1-5</sup>* mutants are indeed caused by lesions in *v100*. The photoreceptor-specific rescue of the ERG further suggests a selectively presynaptic requirement of *V100* (Figure 1B).

*v100* is a highly conserved subunit of the  $V_0$  subcomplex of the vesicular ATPase. Four similar genes (subunits *a1–a4*) exist in *Drosophila*, *C. elegans*, mouse, and human. *Drosophila v100* is more similar to that of the worm, mouse, and human subunit *a1* genes (56%, 58%, and 59%, respectively) than to the other subunits *a2–a4* (Figure 1F).

To determine where *v100* is expressed we performed in situ hybridization. The gene is widely expressed in the embryo and the larval nervous system (Figure 1H). To test if it is required in tissues other than the nervous system, we expressed the full-length cDNA under control of the neuron-specific *elav-GAL4* driver using the GAL4/UAS system (Brand and Perrimon, 1993). Neuron-specific expression of *v100* in mutants rescues lethality and results in viable and fertile adult flies with no obvious behavioral defects. Hence, *v100* is a v-ATPase subunit that is required in the nervous system.

### *Drosophila v100* Partially Rescues Vesicle Trafficking but Not Acidification Defects in Yeast

The v-ATPase subunit *a* is the only component of the v-ATPase encoded by two genes in *S. cerevisiae*, *VPH1* and *STV1*. Vph1p is a vacuolar subunit and Stv1p resides within the Golgi/endosomal compartments (Kawasaki-Nishi et al., 2001; Perzov et al., 2002). While vacuolar fusion has been shown to require Vph1p, acidification persists in the  $\Delta VPH1$  mutant due to compensatory Stv1p function (Bayer et al., 2003; Perzov et al., 2002).

We tested the ability of *Drosophila V100* to rescue defects in a  $\Delta VPH1, \Delta STV1$  double-mutant yeast strain. The double mutant is nonviable on medium at pH 7.5, but can grow at pH 5.5. We therefore tested the ability of *v100* to rescue the lethality at pH 7.5, using the rescue with yeast *VPH1* as a positive control. As shown in Figure 2A, viability was not rescued with *Drosophila v100* at pH 7.5. This result indicates that *v100* cannot rescue the acidification defect in yeast.

In addition to the acidification defect,  $\Delta VPH1, \Delta STV1$  double-mutant yeast are also defective in vesicle endocytosis and trafficking as shown in pulse chase experiments with FM4-64 (Perzov et al., 2002). FM4-64 is a lipophilic dye commonly used to study vesicle trafficking. Wild-type yeast endocytose and transport the dye within minutes from the plasma membrane to the vacuole (Perzov et al., 2002). We performed pulse chase experiments at both pH 5.5 and pH 7.5 with double mutants transformed with control vector, *VPH1*, or the experimental vector carrying *v100* (Figures 2B–2H). To quantify the translocation of the dye from the plasma membrane to the vacuole, we imaged the cells every

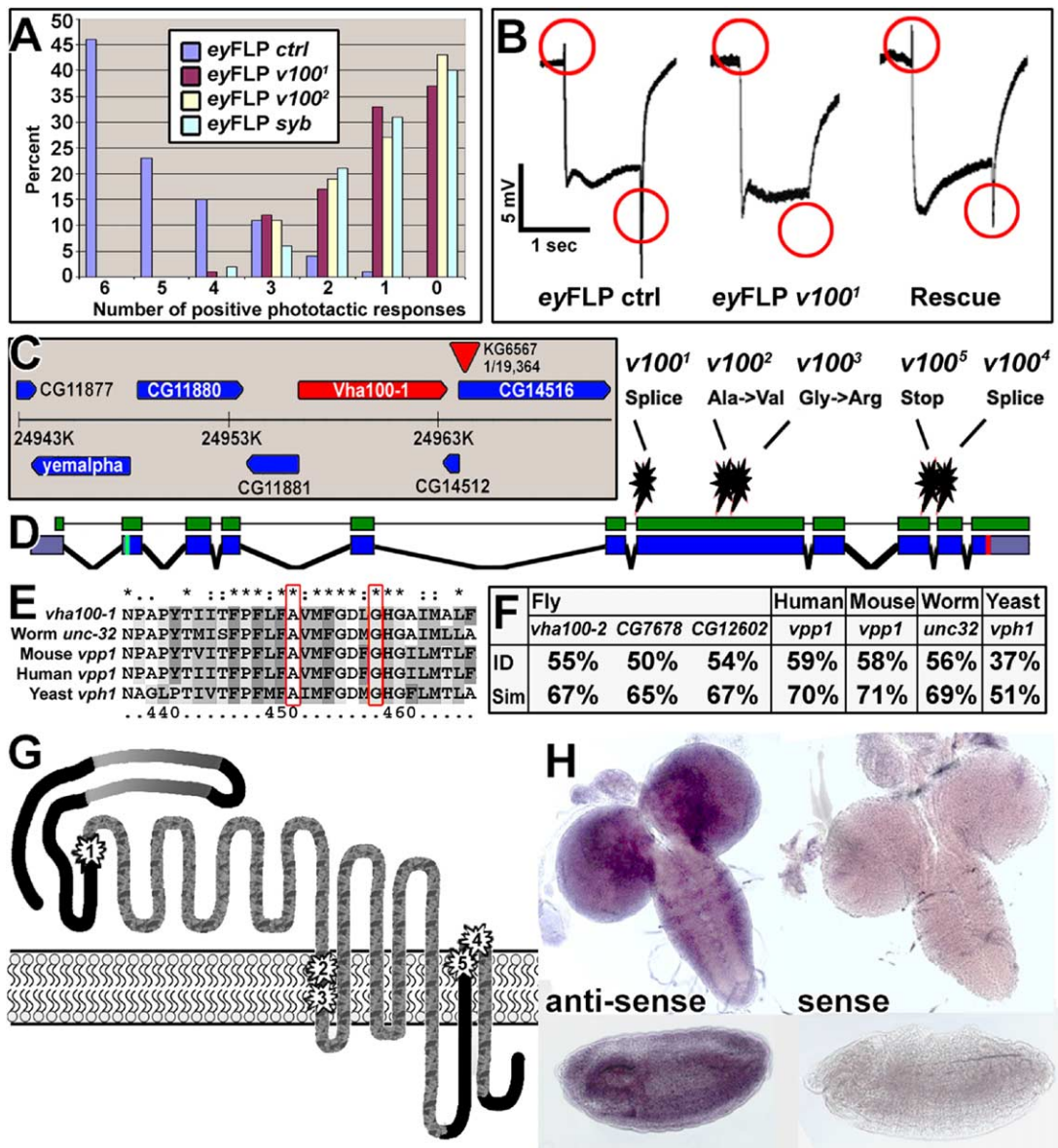


Figure 1. Isolation, Identification, and Presynaptic Rescue of Mutations in *v100*

(A) Phototaxis of eyFLP control, *v100*<sup>1</sup>, *v100*<sup>2</sup>, and *n-syb* flies using the counter-current Benzer assay.

(B) Electrophysiological recordings. eyFLP *v100* mutants lack “on” and “off” transients (red circles), indicative of a failure to evoke a postsynaptic response. Photoreceptor-specific expression of *v100* in an eyFLP *v100* mutant background restores both “on” and “off.”

(C) Twenty-seven kilobyte genomic region containing the P element found to be closest to the lethal mutations using recombination mapping (KG6567, recombination rate 1/19,364).

(D) Identified point mutations of five alleles. CG1709-RC annotation shown in blue; cDNA used for the rescue experiments shown in green.

(E) The protein sequence containing the point mutations of *v100*<sup>2</sup> and *v100*<sup>3</sup> is highly conserved.

(F) Protein sequence homology of V100 with the fly subunits a2–a4 and the human, mouse, worm, and yeast subunit a1 homologs.

(G) V100 predicted protein structure. The N terminus is cytosolic and contains two coiled-coil domains (gray gradients). The protein has seven or nine transmembrane domains (TMDs), depending on the transmembrane prediction algorithm. Depicted are seven TMDs; the two other possible TMDs are the loops depicted between TMD 2/3 and 4/5. The point mutations of the *v100* alleles are marked 1–5. The protein sequences predicted to be deleted in the mutant splice variants is marbled.

(H) In situ hybridizations of third instar larval brains (top) and stage-15 embryos (bottom). Antisense staining on the left shows strong nervous system expression. The sense control is shown on the right.

15 min using confocal microscopy and quantified the ratio of fluorescence intensity on the vacuole to that on the plasma membrane (compare intracellular peaks [arrowheads] with outer membrane [arrows] in Figures

2C–2H and Figure S1 in the Supplemental Data available with this article online). Transport of FM4-64 to the vacuole was significantly accelerated by V100 when compared to the mock-transfected control ( $p < 0.005$ ),

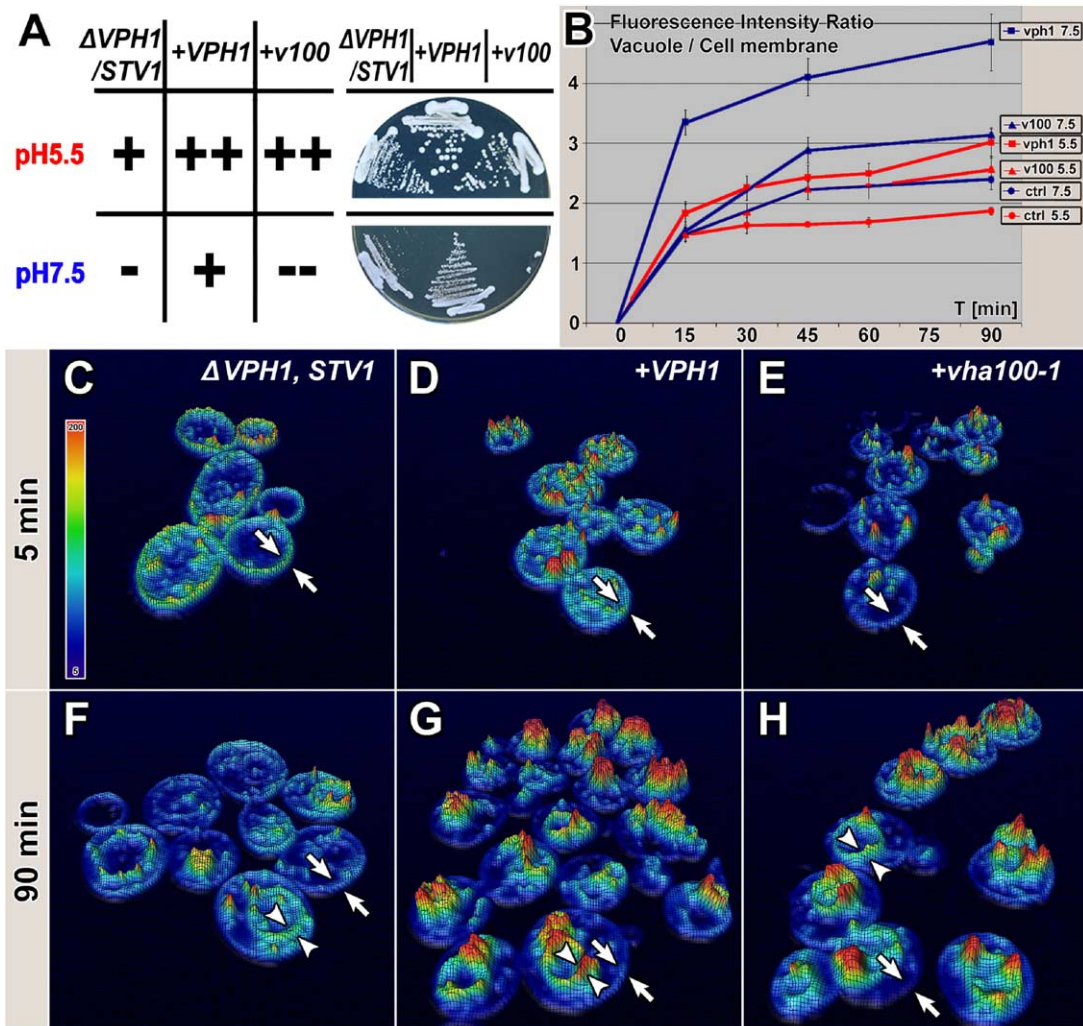


Figure 2. *Drosophila* V100 Rescues Vesicle Trafficking, but Not an Acidification Defect in Yeast

(A) Growth of  $\Delta VPH1, \Delta STV1$  double-mutant yeast expressing a mock control vector, yeast *VPH1*, or fly *v100* at pH 5.5 and pH 7.5. Qualitative growth evaluation on the left; original plates on the right. Note that only rescue with *VPH1* allows normal growth at pH 7.5.

(B) FM4-64 pulse chase experiments with the yeast strains described in (A). Depicted is the ratio of fluorescence intensity on the vacuole compared to fluorescence intensity on the cell membrane. Note that all mutants exhibit translocation of FM4-64 to the vacuole, however with significantly different kinetics. Error bars are SEM.

(C–H) 3D-Hightfield visualization of the 5 min and 90 min time points for all three genotypes in the experiment performed at pH 5.5 quantified in (B). Fluorescence intensity is visualized as relief and color-coded using the color map shown in (C). FM4-64 fluorescence on the outer membrane is marked between arrows; intracellular fluorescence on the vacuole is marked between arrowheads.

although below the Vph1p levels (Figure 2B) at both pH 5.5 and pH 7.5. Taken together, these experiments indicate that V100 can partially compensate for an in vivo endocytosis and vesicle trafficking defect, but not the acidification defect of  $\Delta VPH1, \Delta STV1$  yeast.

#### *v100* Mutant Synapses Contain Increased Vesicle Numbers

Loss of *v100* does not affect photoreceptor viability, development, or their ability to respond to a light stimulus with normal depolarization. These data clearly suggest a lack of general defects in acidification of intracellular compartments or membrane trafficking in these mutants. Hence, the *v100* defects indicate a specific impairment in synaptic transmission. Such defects are

often associated with ultrastructural defects in synaptic vesicle number and/or shape. To assess synaptic vesicle numbers we performed transmission electron microscopy (TEM) of the first optic neuropil, the lamina. We made use of the eye-specific *ey3.5FLP* system (Iris Salecker, personal communication; Mehta et al., 2005) to selectively render the presynaptic photoreceptor terminals homozygous mutant in the brain and carried out TEM for four different mutant alleles. As shown in Figures 3A and 3B, photoreceptor projections in the brain of *ey3.5FLP v100* mutants do not display obvious defects. However, in the lamina, some aggregates and a subtle localization defect of the photoreceptor-specific cell adhesion molecule Chaoptin (mAb 24B10) can be observed (Figures 3C and 3D). The photoreceptor neu-

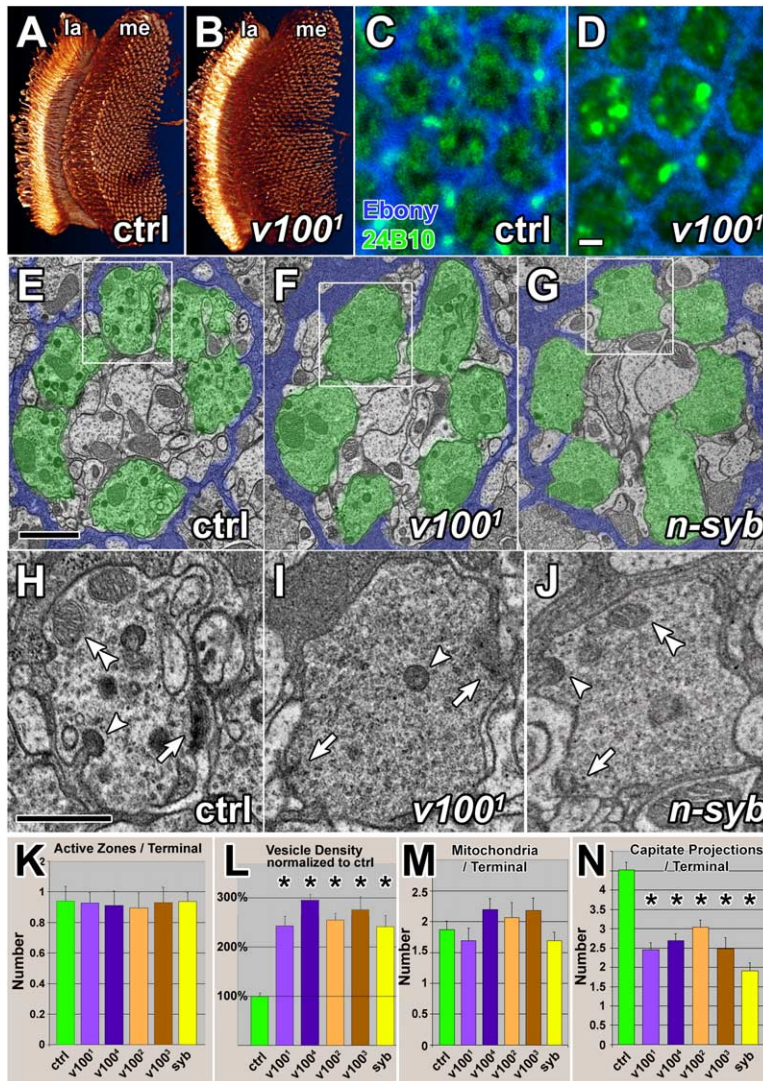


Figure 3. Ultrastructural Analysis of Mutant Photoreceptor Terminals in the Lamina

(A) 3D visualization of control photoreceptor neurons stained with mAb 24B10. la: lamina; me: medulla.

(B) Visualization of *v100<sup>1</sup>* mutant photoreceptor neurons as in (A) projecting into a heterozygous control brain.

(C) Cross-section through a control lamina, showing the hexagonal pattern of cartridges, synaptic units that are demarcated by epithelial glia (blue) and contain the presynaptic photoreceptor terminals (green).

(D) Lamina cross-section containing *v100<sup>1</sup>* mutant photoreceptor terminals. The overall cartridge structure is unaltered. Scale bar in (D) for (C)–(D): 2  $\mu$ m.

(E–G) TEM micrographs of cartridges containing control, *v100<sup>1</sup>*, and *n-syb* mutant terminals, respectively. Demarcating glia are colored blue and photoreceptor terminals green to accentuate the structures. Scale bar in (E) for (E)–(G): 1  $\mu$ m.

(H–J) Individual terminals that are boxed in (E)–(G). Arrows: active zones; arrowheads: capitate projections (glial invaginations); double arrowheads: mitochondria. Scale bar in (H) for (H)–(J): 500 nm.

(K–N) Quantification of organelles. Both *v100<sup>1</sup>* and *n-syb* mutant terminals exhibit an increase in vesicle density of about 2.5-fold and a reduced number of capitate projections. Error bars are SEM.

rons R1–R6 that are responsible for synaptic transmission assayed in the ERG terminate in the lamina (Meinertzhagen and Hanson, 1993). The lamina is a structured array of 700–800 cartridges. In each cartridge, the dendritic projections of postsynaptic cells are surrounded by six photoreceptor terminals (green in Figures 3E–3G). As shown in Figures 3C and 3D and Figures 3E and 3F, cartridges containing *v100<sup>1</sup>* mutant photoreceptor terminals appear normally organized. However, *v100* mutant terminals exhibit an ~2.5-fold increase in vesicle density compared to control ( $p < 0.0001$ ; Figure 3L). In addition, we found a reduction in the number of capitate projections, dynamically active invaginations of the surrounding epithelial glia that have been associated with vesicle endocytosis ( $p < 0.001$ ; Figure 3N; arrowheads in Figures 3H–3J). Some mutant terminals appear to be enlarged (data not shown). In contrast, the numbers of active zones and mitochondria per terminal are unaltered in mutants (Figures 3K and 3M; arrows and double-arrowheads in Figures 3H–3J). These defects are similar to the phenotypes associated with loss of the neuronal vesicle-SNARE *n-syb* which is required for vesicle priming and fusion (Broadie et al., 1995;

Deitcher et al., 1998; Hiesinger et al., 1999). To compare the phenotypes associated with loss of *n-syb* to those of *v100*, we also performed TEM on *n-syb* mutant terminals. Loss of *n-syb*, like the loss of *v100*, causes embryonic lethality and loss of “on” and “off” transients in eyFLP mosaics (Deitcher et al., 1998; data not shown). *n-Syb* was further shown to cause an increased number of vesicles at the embryonic neuromuscular junction (NMJ; Broadie et al., 1995). As shown in Figures 3G and 3J and 3K–3N, TEM on laminae of *n-syb* null photoreceptor terminals exhibited a similar phenotype to *v100* mutant terminals: increased vesicle density, reduced number of capitate projections, and normal numbers of active zones and mitochondria. In summary, the TEM phenotypes indicate a specific defect in *v100* mutant terminals that leads to an accumulation of vesicles that is very similar to the v-SNARE *n-syb* mutant phenotype.

#### V100 Is Enriched in Synaptic Terminals at Active Zones

To investigate the V100 protein localization, we generated a polyclonal antibody against amino acids 1–416.

Anti-V100 immunoreactivity is abundant in the neuropils of the adult brain but is also present in cell bodies (Figure 4A). In the lamina, anti-V100 stains cartridges in a donut-like pattern characteristic of the presynaptic photoreceptor terminals, similar to Synaptotagmin (Syt), a synaptic vesicle marker (Figures 4B–4D). As much of the characterization of the *v100* mutant phenotypes was carried out at the NMJ, we investigated the protein localization in wild-type and mutant embryos (22–24 hr). As shown in Figures 4E–4J, the V100 protein is enriched at the embryonic NMJ and in the neuropil of the central nervous system (CNS). Protein levels in *v100<sup>1</sup>/Df* and other mutant combinations in the CNS neuropil as well as NMJ staining are strongly reduced to a weak punctate staining that is found in all tissues, including control animals (Figures 4K–4N and S2). This suggests that there is either residual protein or some minor nonspecific component that is recognized by the antiserum. In summary, V100 is enriched at synaptic terminals in the embryonic and adult CNS as well as at the NMJ.

All *v100* mutations develop as morphologically normal L1 larvae that fail to hatch. When dissected out of the egg case, they do not exhibit contraction waves that progress from anterior to posterior but rather show uncoordinated twitching. The immobile late embryos/early L1 larvae live for approximately 24–48 hr but cannot be kept alive longer using fluid yeast. To determine if there are morphological defects at the NMJs or aberrant localization of known synaptic markers, we stained NMJs using antibodies against cell adhesion molecules (HRP, Fas2), synaptic vesicle markers (Syt, Cysteine String Protein, n-Syb), target SNAREs (Syntaxin [Syx], SNAP-25), active zone markers (nc82, DPAK) and post-synaptic receptors (GluRII). We did not observe any obvious morphological defects or aberrant protein localization of the analyzed markers (Figures 4K–4N, S2, 7A–7F, S4I–S4N, and data not shown). Hence, *v100* is either not required for embryonic development or a maternal protein or RNA contribution to the egg is responsible for normal development. We therefore generated maternal knockout (MKO) embryos for *v100<sup>1</sup>* and *v100<sup>2</sup>* (Chou and Perrimon, 1992). These embryos display no developmental delay and present the same behavior and morphology as all other mutant allelic combinations (data not shown). In summary, these data indicate that embryonic and NMJ development does not depend on the presence of *v100*.

To define V100 localization inside synaptic boutons at high resolution, we analyzed the colocalization of V100 with vesicle and active zone markers at the L3 larval NMJ using 3D deconvolution of confocal image stacks (see Supplemental Experimental Procedures). These boutons are typically 3–6  $\mu\text{m}$  in diameter. V100 staining inside boutons colocalizes mostly with the vesicle marker Syt (Figures 4O and 4R). However, we consistently observed an increased V100 staining at active zones labeled with mAb nc82 (Wucherpfennig et al., 2003; arrowheads in Figures 4O–4R). A quantitative colocalization analysis revealed significantly more colocalization of V100 with nc82 than Syt with nc82, indicating an enrichment of V100 relative to Syt at active zones (Figures 4S–4X). We further analyzed V100 protein content in a vesicle preparation versus membrane frac-

tion (Schulze et al., 1995). V100 is enriched in the vesicle fraction but is also present in the membrane fraction containing both vesicles and presynaptic membranes (Figure S3). These data indicate that V100 is a synaptically enriched protein that localizes to both synaptic vesicles and active zones.

#### V100 Interacts with t-SNAREs

V100 homologs have previously been shown to interact with SNARE proteins in yeast and vertebrates (Bennett et al., 1992; Galli et al., 1996; Morel, 2003; Peters et al., 2001), and V100 contains two N-terminal coiled-coil domains (coil 1, 44–75; coil 2, 90–135) that may interact with SNARE proteins. We therefore investigated V100 interactions with SNAREs. First, we tested bacterially produced V100 protein domains that lack the transmembrane regions in GST pull-down assays. As shown in Figure 5A, both GST-V100 and GST-Syx retrieve His-tagged SNAP-25. Furthermore, GST-V100 also interacts with His-Syx. In contrast, only GST-Syx, but not GST-V100, pulls down His-n-Syb, indicating that V100 directly interacts with Syx and SNAP-25, the SNAREs at the target membrane, but not with the vesicle-SNARE n-Syb. We then reversed the experiment using GST-Syntaxin to pull down a His-tagged V100 N-terminal fragment of 133 amino acids (amino acids 10–143) containing the two coiled-coil domains (Figure 1G). Syx also pulled down this V100 fragment, indicating an N-terminal Syx interaction domain (Figure 5B).

To confirm these interactions, we verified the pull-down results with coimmunoprecipitation assays. Beads were coated with purified IgGs extracted from anti-V100 antiserum and tested for the ability to immunoprecipitate Syx or SNAP-25, either alone or in combination with V100. Consistent with the pull-down results, both Syx and SNAP-25 can be immunoprecipitated in the presence of V100 (Figure 5C). Finally, we tested anti-Syx-coated beads for their ability to coimmunoprecipitate native V100 from fly head extract. As shown in Figure 5D, both Syx and V100 are coimmunoprecipitated from head extract (that was cleared of insoluble material and membrane fragments) with anti-Syx coated beads, indicating that they exist at least partially as a complex in vivo (Figure 5D). In summary, these results indicate that V100 and the t-SNAREs SNAP-25 and Syx directly interact.

The in vivo significance of the V100–Syx interaction is supported by the results of a suppressor screen carried out in parallel to our original eyFLP screen. Overexpression of Syx driven by GMR-Gal4 in photoreceptors at low levels (in flies reared at 18°C) causes a rough eye phenotype and high levels of Syx (28°C) cause cell death. We reasoned that loss of a protein required for Syx action may suppress this toxic effect and screened 181 mutants isolated on chromosome arm 3R in the eyFLP screen (Mehta et al., 2005) for suppression of the rough eye phenotype. Eight mutants displayed suppression, two of which are *v100<sup>1</sup>* and *v100<sup>4</sup>*, severe loss-of-function alleles (Figures 5E–5J). In contrast, mutations causing single-amino acid changes in the first transmembrane domain, *v100<sup>2</sup>* and *v100<sup>3</sup>*, displayed no suppression (data not shown). This result indicates that overexpressed Syx requires the function of

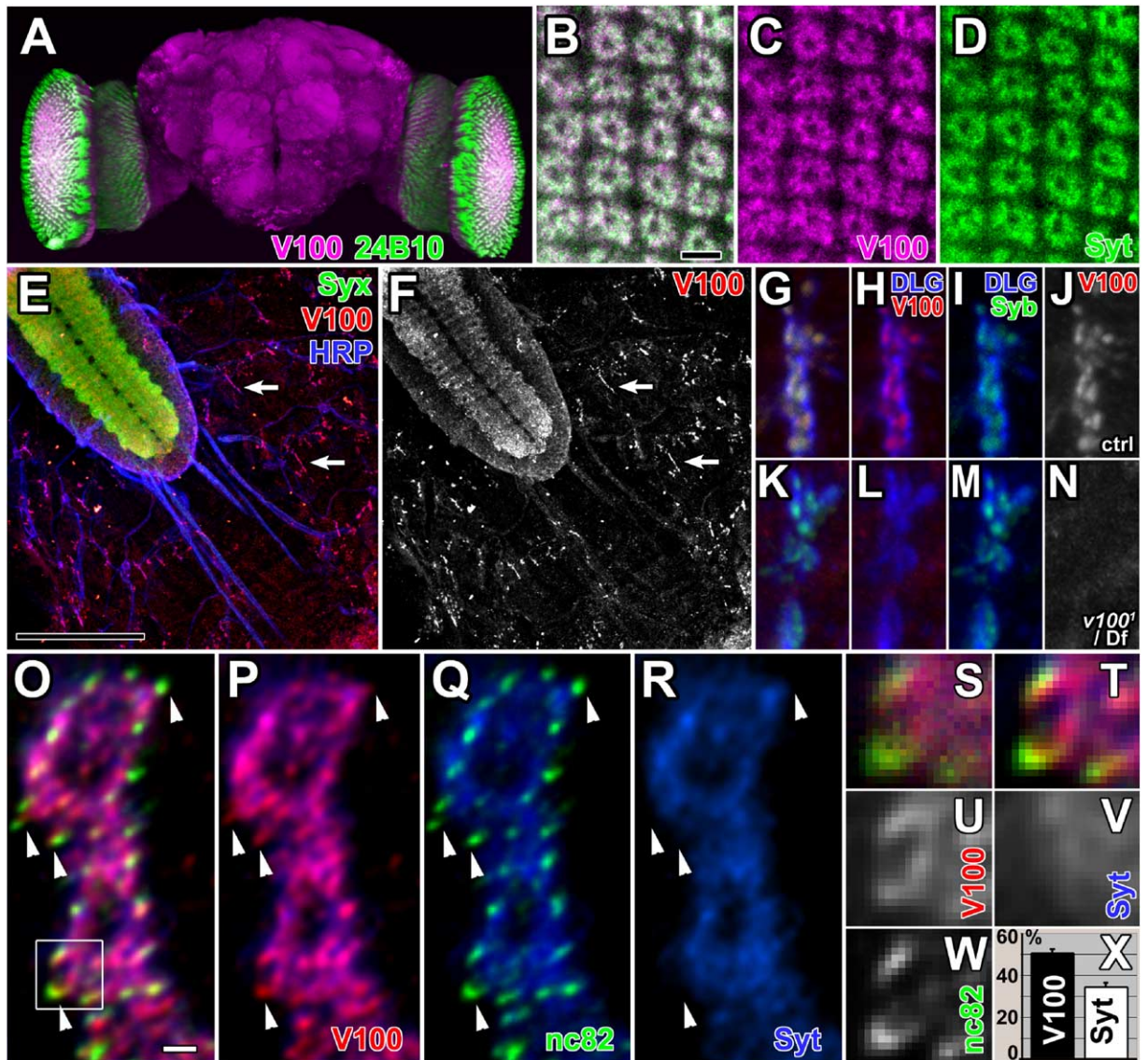


Figure 4. Synaptic Localization of V100

(A) Adult whole-mount brain 3D visualization. V100 staining in the neuropils and cell bodies is shown in magenta. Photoreceptor-specific staining with mAb 24B10 is shown in green. The laminae are cut open on both sides revealing cross-sections of these synaptic structures. (B–D) High-resolution confocal scans of lamina cross-sections. Note the donut-like shape of V100 (magenta) and Syt (green) staining, characteristic of the localization of presynaptic photoreceptor terminals in cartridges (compare TEM of cartridges in Figure 3). Scale bar: 5  $\mu$ m. (E and F) Fillet of a stage-17 embryo exposing the CNS (top left) and synapses on the body wall musculature. Green: Syx; red: V100; blue: HRP. The V100 channel is separately shown in (F). Arrows: NMJs at muscle 6/7. Scale bar: 50  $\mu$ m. (G–J) High-resolution confocal scan of a control embryonic NMJ on muscle 4. DLG (blue) demarcates the NMJ border, whereas V100 (red) and n-Syb (green) colocalize presynaptically. The V100 channel is shown separately in (J). (K–N) High-resolution confocal scan of a *v100<sup>1</sup>/Df* embryonic NMJ on muscle 4. The staining is identical to that in (G)–(J) except that V100 staining is reduced to background levels. The V100 channel is shown separately in (N). (O–R) High-resolution 3D-deconvolved confocal sections of muscle 6/7 boutons at the third instar larval NMJ. Green: active zones labeled with mAb nc82; red: V100; blue: vesicles labeled with anti-Syt. Most V100 staining colocalizes with Syt but also extends beyond Syt at active zones (arrowheads). Scale bar: 1  $\mu$ m. (S–W) Boxed region of (O) shown without pixel interpolation at original pixel size of 90  $\times$  90 nm. (S) and (T) are three-channel composites before and after 3D deconvolution. The three channels are shown separately in (U)–(W). (X) Quantification of V100 and Syt fluorescence in five independent 3D-deconvolved datasets in threshold-segmented nc82-stained domains (shown as percentage of nc82 staining overlap). Note that V100 exhibits 50% more colocalization with the active zone marker nc82 than Syt. Error bars are SEM.

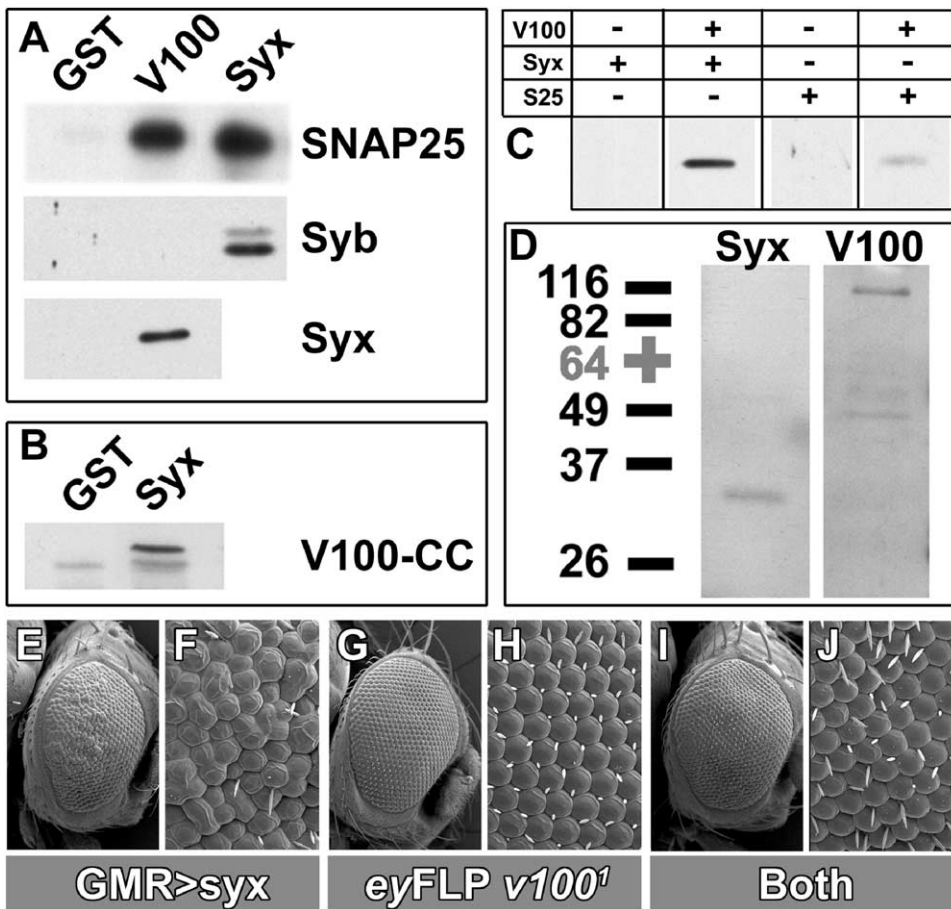


Figure 5. V100 Interacts with SNAREs

(A) GST pull-down assays. Top: GST (negative control), GST-V100, and GST-Syx. SNAP-25, Syb, and Syx indicate His-tagged recombinant proteins as well as the antibodies used to probe the Western blots. All fusion proteins are lacking transmembrane domains.  
 (B) GST pull-down assay using GST-Syx to pull down a His-tagged N-terminal domain containing the two coiled-coils of V100 (V100-CC).  
 (C) Coimmunoprecipitation (CoIP) experiments using anti-V100 coated beads. Addition of mixtures of recombinant V100 and Syx or V100 and SNAP-25, but not Syx or SNAP-25 alone, can be immunoprecipitated.  
 (D) CoIP experiment from fly head extract using anti-Syx-coated beads. Syx as well as native full-length V100 are immunoprecipitated.  
 (E and F) Scanning electron microscopic (SEM) images of a fly eye with photoreceptor-specific (GMR-Gal4) expression of Syx (genotype: *eyFLP/+; GMR-Gal4, UAS-Syx/+; FRT c1/TM3, Sb*). Overexpression of Syx is toxic and causes developmental defects resulting in a rough-eye phenotype.  
 (G and H) SEM images of an *eyFLP v100<sup>1</sup>* fly eye showing wild-type morphology (genotype: *eyFLP/+; +/CyO; FRT c1/FRT v100<sup>1</sup>*).  
 (I and J) SEM images of an *eyFLP v100<sup>1</sup>* fly eye with photoreceptor-specific Syx expression show suppression of the Syx overexpression toxicity (genotype: *eyFLP/+; GMR-Gal4, UAS-Syx/+; FRT c1/FRT v100<sup>1</sup>*).

V100 to be fully toxic and provides some genetic evidence that V100 acts downstream of Syx, in agreement with observations in yeast (Peters et al., 2001). The biochemical data further suggest that this function is mediated by a direct interaction between the two proteins.

#### Neurotransmitter Release Is Impaired at *v100* Mutant Synapses

To test a possible role of *v100* instead of or in addition to synaptic vesicle acidification, we evaluated synaptic function at the embryonic NMJ. We first investigated miniature excitatory postsynaptic currents (mEPSCs), i.e., spontaneous neurotransmitter release events. If loading of vesicles with neurotransmitter is impaired two possibilities arise. (1) The size of the mEPSCs may

be smaller due to a lower concentration of neurotransmitter in the vesicles. (2) If vesicle loading is an all-or-none process, the frequency of mEPSCs may be reduced in the mutants to reflect fusion of empty vesicles. As shown in Figures 6A and 6B, the mean size of the mEPSCs is not significantly different in the mutants relative to control. Furthermore, the distribution of the mEPSC amplitudes pooled across different cells and animals are not significantly different in both mutants and control (Kolmogorov-Smirnov tests—*v100<sup>2</sup>/v100<sup>3</sup>* versus ctrl,  $p = 0.59$ ; *v100<sup>1</sup>/Df* versus ctrl,  $p = 0.67$ ; *v100<sup>1</sup> MKO/Df* versus ctrl,  $p = 0.73$ ). The frequency of mEPSCs is more variable but on average similar to wild-type in the heterozygous allelic combination of two missense mutations, *v100<sup>2</sup>* and *v100<sup>3</sup>*. However, we

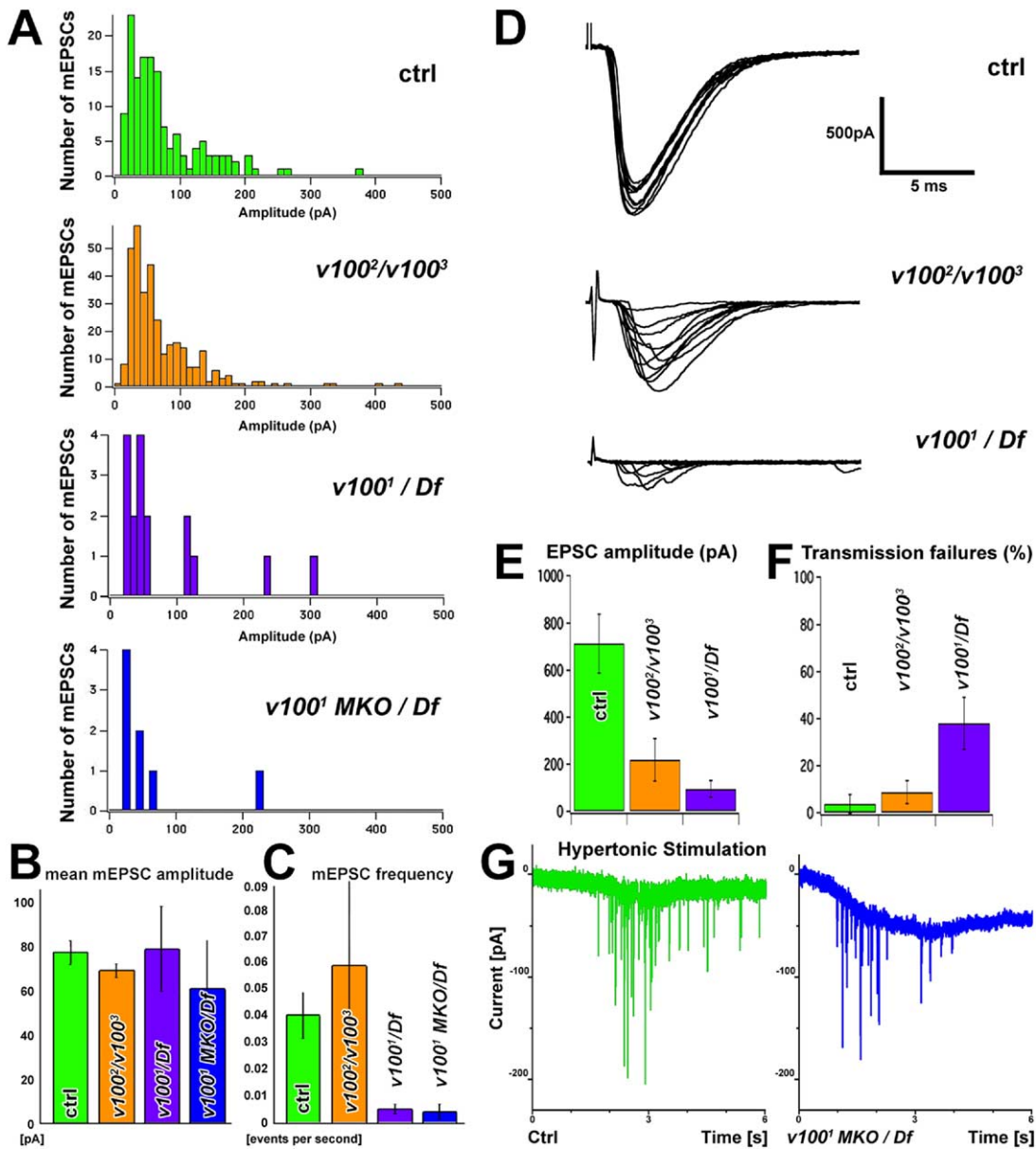


Figure 6. Electrophysiological Analysis of  $v100$  Alleles at the Embryonic NMJ

(A) Distribution of miniature excitatory postsynaptic currents amplitudes in control (green),  $v100^2/v100^3$  (orange),  $v100^1/Df$  (violet), and  $v100^1 MKO/Df$  (blue). Note that the number of events analyzed is much lower in  $v100^1/Df$  and  $v100^1 MKO/Df$  because mEPSCs are rare.

(B) The mean amplitude of mEPSCs in all four genotypes shows no significant difference. ctrl:  $77.48 \pm 5.34$  (n = 161),  $v100^2/v100^3$   $69.15 \pm 3.19$  (n = 330),  $v100^1/Df$   $79.29 \pm 19.23$  (n = 16),  $v100^1 MKO/Df$   $60.93 \pm 23.91$  (n = 7). All error bars are SEM.

(C) The frequency of mEPSCs is strongly reduced in  $v100^1/Df$  and  $v100^1 MKO/Df$  compared to control.  $v100^2/v100^3$  NMJs display an mEPSC frequency that is on average not significantly different from control but show higher variability (note size of error bars). ctrl  $0.041 \pm 0.009$  (n = 15),  $v100^2/v100^3$   $0.060 \pm 0.035$  (n = 13),  $v100^1/Df$   $0.005 \pm 0.002$  (n = 6),  $v100^1 MKO/Df$   $0.004 \pm 0.003$  (n = 6). All error bars are SEM.

(D) Representative evoked responses (EPSCs) at the embryonic NMJ.

(E) EPSC amplitude is significantly reduced in both  $v100^2/v100^3$  and  $v100^1/Df$ .

(F)  $v100^1/Df$  but not  $v100^2/v100^3$  show a significant number of transmission failures upon stimulation.

(G) Hypertonic stimulation using a 3 s application of 850 mM sucrose. Shown are control (green) and the strongest allelic combination  $v100^1 MKO/Df$  (blue). Hypertonic release exists in all genotypes, albeit at a reduced level in the mutants. The mean amplitude of release events is not significantly different between control and mutant (see Figure S4).

did observe a significant reduction ( $p < 0.05$ ) in mEPSC frequency in the allelic combination  $v100^1/Df$  (Figure 6C). To test the contribution of maternally contributed  $v100$ , we measured spontaneous release in  $v100^1 MKO/$

$Df$  embryos that were deficient in maternally contributed  $v100$  protein or mRNA. In these animals, we saw no reduction in mEPSC amplitude but a very severe reduction in mEPSC frequency (very similar to the one for

$v100^1/Df$ ) relative to control ( $p < 0.05$ ). These results suggest that in late-stage embryos that have lost the zygotic contribution, the maternal component has largely disappeared. In summary, our mEPSC analysis indicates that neurotransmitter content is normal in vesicles. However, it leaves open the question whether the reduced mEPSC frequency is a result of the fusion of empty vesicles or an impairment of the fusion process itself.

Since mutant synapses contain loaded vesicles that can be released spontaneously, the defect at the photoreceptor synapse as well as the lack of coordinated movements in the late embryo may be explained by aberrant evoked neurotransmitter release. To test this possibility, we examined EPSCs at the neuromuscular junction evoked by stimulation of the motor nerve supplying muscle 6. As shown in [Figures 6D and 6E](#), we recorded a significant reduction in the mean EPSC amplitudes ( $p < 0.01$ ) from  $712.7 \pm 125$  pA (SEM;  $n = 15$ ) in control to  $218.3 \pm 90$  pA ( $n = 8$ ) in  $v100^2/v100^3$  mutant embryos.  $v100^1/Df$  mutants exhibit an even more severe phenotype as the mean evoked amplitude is only  $94.6 \pm 36$  pA ( $n = 9$ ;  $p < 0.001$ ). Furthermore,  $v100^1/Df$  synapses display a marked increase in transmission failures:  $31.1\% \pm 10.5\%$  relative to  $3.3\% \pm 3.3\%$  ( $p < 0.005$ ) in control animals ([Figure 6F](#)). There was no significant difference between the failure rate of  $v100^2/v100^3$  and wild-type. These data indicate a strong impairment of the synapse to release vesicles upon nerve stimulation. The normal mEPSC size and frequency in  $v100^2/v100^3$  mutants combined with a significantly reduced evoked response in this allelic combination argue against a defect in vesicle acidification: if the reduction in the evoked response were due to the release of empty vesicles (“shooting blanks”), these unloaded vesicles should be reflected in an equally reduced frequency of spontaneous release events. Therefore, the reduction in evoked release is likely to be due to a reduction in the number of vesicles released per stimulus. This effect may be due to a reduced presynaptic  $Ca^{2+}$  signal, a reduction of the readily releasable pool of synaptic vesicles, or an impairment in the fusion process. We tested these possibilities using a  $Ca^{2+}$ -independent stimulation paradigm ([Rosenmund and Stevens, 1996](#)) by pressure application of a 3 s pulse of hypertonic sucrose solution (850 mM) at the NMJ in the presence of 1  $\mu$ M TTX. We detected postsynaptic currents in response to hypertonic solution in wild-type and mutant ( $v100^2/v100^3$  and  $v100^1/Df$ ) animals (data not shown). Furthermore, we tested maternal knockout  $v100^1$  MKO/ $Df$  embryos (the most severe allelic combination) in the presence of reduced  $Ca^{2+}$  (0.5 mM), and we also observed a response with hypertonic solution, indicating that loaded vesicles are docked and can be released in a  $Ca^{2+}$ -independent manner ([Figure 6G](#)). However, we observed fewer responses in mutants than in wild-type. Importantly, the average amplitude of individual events in control and maternal knockout  $v100^1$  MKO/ $Df$  embryos is not significantly different (Kolmogorov-Smirnov test,  $p = 0.94$ ; [Figure S4](#)). These data indicate that the boutons contain vesicles that are loaded with neurotransmitter and that vesicles can be released by hypertonic stimulation. They also argue that the SNAREs are functional and that vesicles can be primed for re-

lease. In addition, our data do not suggest a defect in vesicle acidification. We therefore argue that V100 is required for synaptic vesicle fusion.

### FM1-43 Uptake Is Impaired at $v100$ Mutant Synapses

It has previously been shown that vesicle acidification does not impair uptake of FM1-43 in cerebellar granule cells ([Cousin and Nicholls, 1997](#)), in rat hippocampal neuronal slices ([Zhou et al., 2000](#)), and at *Drosophila* third instar larval NMJs ([Kuromi and Kidokoro, 2000](#)). These studies imply that defective vesicle acidification does not affect synaptic vesicle cycling. Hence, FM1-43 uptake should be normal if  $v100$  mutants were selectively defective in synaptic vesicle acidification. However, if vesicles fail to be released, as indicated by the electrophysiological data, FM1-43 uptake should be impaired. To measure FM1-43 uptake at mutant embryonic NMJs, we developed a new quantitative protocol using the fixable FM1-43FX dye (see [Experimental Procedures](#)).

We first labeled NMJs with FM1-43, obtained 3D confocal datasets, and quantified the fluorescence of NMJs of 33 embryo fillets of unstimulated controls. We found an average ratio of FM labeling inside (boutons) to outside (muscle) of 1.55, indicating that the membranous boutons have a significantly higher affinity for FM1-43 even in the absence of active uptake ([Figures S5C–S5E](#)). The average ratio for stimulated controls ( $n = 47$ ) was found to be 2.23, thus assigning boundaries for minimal and maximal FM uptake ratios ([Figures 7A–7C and 7J](#)).  $v100^1/Df$  and  $v100^2/v100^3$  animals exhibited intermediate ratios of 1.74 ( $\pm 0.08$ ) and 1.62 ( $\pm 0.08$ ), respectively ([Figures 7J and S5I–S5N](#)). These uptake ratios correspond to 10.8% and 29.7% uptake of the stimulated controls. The values are not significantly different from each other but are significantly lower than control ( $p < 0.001$ ). In comparison, *n-syb* null mutant embryos exhibit 44.5% uptake when compared to the stimulated control, which is likewise not significantly different from the  $v100$  mutant embryos but significantly lower than control ( $p < 0.005$ ; [Figures S5F–S5H](#)). These results indicate that vesicle cycling is substantially reduced in both *n-syb* and  $v100$  mutants. To test whether this residual vesicle cycling could be attributed to maternally contributed protein in the  $v100$  mutants, we tested maternal knockout embryos.  $v100^1$  MKO/ $Df$  synapses display 1.8% FM uptake, which is not significantly different from unstimulated controls ([Figures 7D–7F and 7J](#)). Lastly, we asked whether selective disruption of vesicle acidification with Bafilomycin A1 (Baf) affects FM uptake in our paradigm. Baf directly acts on the v-ATPase and blocks proton translocation, thus eliminating the proton motive force and neurotransmitter loading ([Dröse and Altendorf, 1997](#)). We tested the influence of Baf on FM uptake and found no significant deviation from the stimulated control ([Figures 7G–7J](#)), corroborating other studies ([Cousin and Nicholls, 1997](#); [Kuromi and Kidokoro, 2000](#); [Zhou et al., 2000](#)). In summary, our results indicate that  $v100$  mutant synapses display synaptic vesicle cycling defects that are independent of a possible role of V100 in acidification.

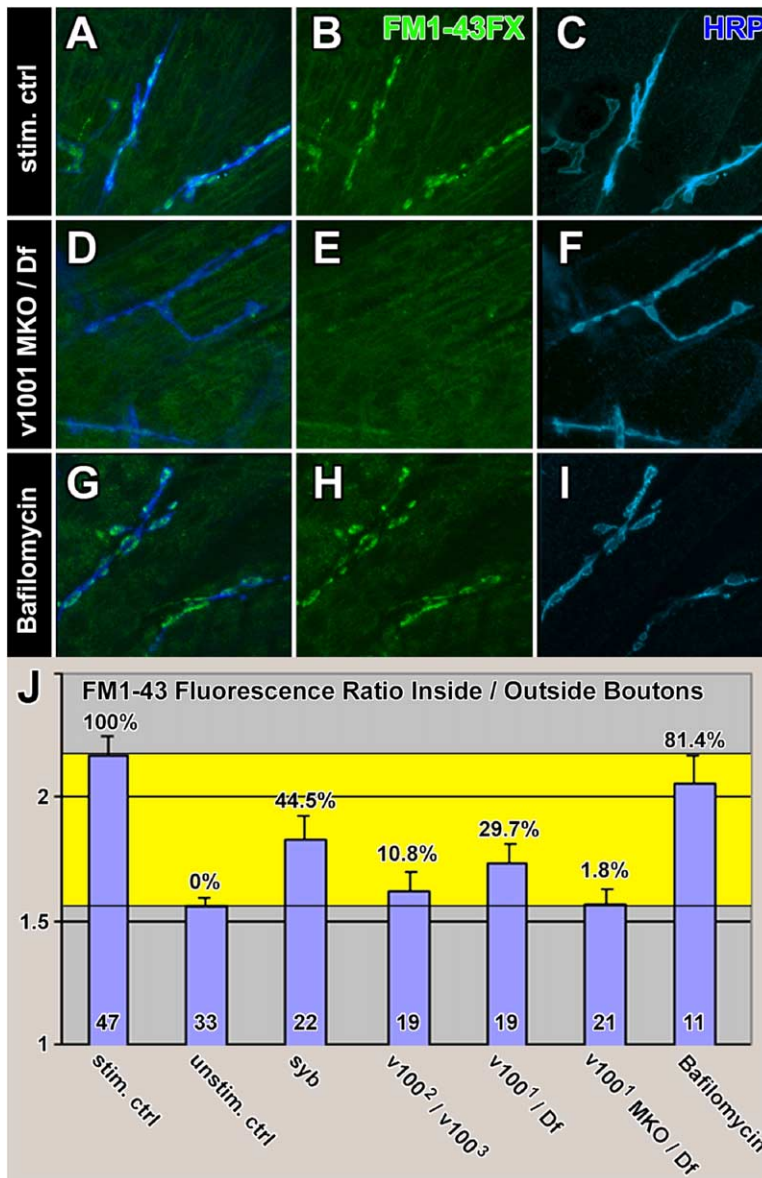


Figure 7. FM1-43 Uptake at the Embryonic NMJ

(A–C) FM1-43FX uptake experiment using a 5 min 30 mM K<sup>+</sup> stimulation paradigm.

(D–F) FM1-43FX uptake using the same stimulation paradigm in a *v100<sup>1</sup>* MKO/Df mutant.

(G–I) FM1-43FX uptake using the same stimulation paradigm after 15 min preincubation with 1 μM Bafilomycin A1 (Baf) as well as 1 μM Baf in the FM1-43 staining solution.

(J) Quantification of FM1-43 uptake experiments in stimulated control (A–C), unstimulated control (Figures S4C–S4E), *n-syb* (Figures S4F–S4H), *v100<sup>2</sup>/v100<sup>3</sup>* (Figures S4I–S4K), *v100<sup>1</sup>/Df* (Figures S4L–S4N), *v100<sup>1</sup>* MKO/Df (D–F), and control with added Baf (G–I). Shown is the ratio of the mean fluorescence intensity of the FM1-43 channel within the boundaries of HRP staining versus muscle background in 3D high-resolution confocal datasets. The yellow area marks the boundaries defined by unstimulated and stimulated control. Percentages of FM1-43 uptake are given with respect to these boundaries. The number of individual embryos analyzed is indicated inside bars. Error bars are SEM.

## Discussion

Here we report the identification of mutations in *v100*, the subunit  $\alpha 1$  of the v-ATPase V<sub>0</sub> complex in *Drosophila*. We present an initial characterization of *v100* mutant phenotypes that is inconsistent with a role of *v100* in acidification only. Our data indicate that V<sub>0</sub> functions in a late step in synaptic vesicle exocytosis.

### The v-ATPase: Acidification and More?

Vesicular or vacuolar ATPases are the most prominent intracellular proton pumps, consisting of at least 12 subunits in two sectors (V<sub>0</sub> and V<sub>1</sub>). Acidification is important for many cellular functions, including receptor-ligand dissociation, degradative pathways, and the generation of intercompartment proton motive forces that are in turn utilized as driving forces for numerous secondary transport processes (Nelson, 2003; Nishi

and Forgac, 2002). Here, we report the consequences of the selective disruption of a V<sub>0</sub> subunit  $\alpha 1$  homolog in neurons. The V<sub>0</sub> subunit  $\alpha$  is encoded by four homologous genes in flies, worms, mouse, and human. The data from yeast and *C. elegans* indicate a crucial role of V<sub>0</sub> subunit  $\alpha$  proteins for specific functions in distinct intracellular compartments and different cell types (Kawasaki-Nishi et al., 2001; Perzov et al., 2002; Oka et al., 2001; Pujol et al., 2001).

We isolated mutations in *v100* based on the specific defect of photoreceptor neurons to evoke a postsynaptic response. Photoreceptors are an excellent “test tube” because they are not required for viability of the fly, and numerous assays can be used to assess morphology and function. Since loss of *v100* does not affect photoreceptor specification, development, viability, and the ability to sense light, we surmise that most intracellular vesicle trafficking and acidification pro-

cesses are unaffected. Indeed, mutations that affect two key protein components of the  $V_1$  subcomplex (subunits A and B) are cell lethal when removed in photoreceptors, and acidification as measured with LysoSensor in *v100* mutant photoreceptor cell bodies is unaffected (P.R.H. and H.J.B., unpublished data). Hence, if acidification is the cause of the observed phenotypes, it is likely to only affect synaptic vesicles.

Several methods can be used to directly or indirectly assess the acidification of synaptic vesicles. The pH-sensitive dye LysoSensor or genetically encoded pHluorin, a pH-sensitive GFP fusion protein that localizes within vesicles, can be used in *Drosophila* neurons to directly assess synaptic vesicle acidification (Miesenböck et al., 1998). Unfortunately, the intensity differences at embryonic NMJs are too small to be observed with our confocal system (P.R.H. and H.J.B., unpublished data). However, several lines of evidence allow us to assess the contribution of a possible acidification defect to the observed phenotypes. We find that several results are not consistent with a defect in synaptic vesicle acidification alone. These include (1) the accumulation of vesicles in mutant terminals, (2) the normal mEPSC amplitude and frequency combined with a severely reduced evoked response in a hypomorphic allelic combination, and (3) the impairment of FM1-43 uptake. In addition, several lines of evidence are not readily explained with the function of V100 as part of a proton pump: (1) selective partial rescue of vesicle trafficking but not acidification in yeast, (2) selective interaction with t-SNAREs, and (3) localization at active zones. Taken together, our results indicate that V100 exerts additional or alternative functions to synaptic vesicle acidification at *Drosophila* synapses.

#### SNAREs and $V_0$ : Fusion of “Proximity” and “Pore”?

The hypothesis that SNAREs form the basic molecular apparatus that forces lipid bilayers to fuse is widely supported (Jahn, 2004; Sørensen, 2004). However, this does not imply that SNAREs alone are required to induce synaptic vesicle exocytosis. SNAREs alone are sufficient to induce fusion of liposomes, but the kinetics of these events does not mimic the kinetics that has been observed in synaptic vesicle fusion in vivo (Hu et al., 2003; Weber et al., 1998). The yeast vacuolar fusion assay is the only system in which evidence for an additional component downstream of SNARE function has been identified (Peters et al., 2001; Bayer et al., 2003). Interestingly, Israëli et al. (1986) reported the isolation of a proteolipid pore complex from synaptosomes from electroplaques of *Torpedo*, named the “mediatophore.” This pore complex was later shown to contain a subunit of the  $V_0$  complex and transfection of this component in some cells allowed quantal release of neurotransmitter (Falk-Vairant et al., 1996; Morel, 2003). Subunit a1 was recently shown to localize to synaptic terminals and interact with the v-SNARE n-Syb (Morel et al., 2003). While the localization is in agreement with our findings at *Drosophila* synapses, we found selective interactions of V100 with the t-SNAREs Syx and SNAP-25 in agreement with the observations made in yeast (Peters et al., 2001).

Our analyses reveal many similarities between *v100*

and *n-syb* mutants: both die as late embryos without coordinated movement, accumulate vesicles at synapses, exhibit reduced spontaneous vesicle release and FM1-43 uptake, contain vesicles with normal transmitter content that is poorly released upon stimulation, and interact with t-SNAREs. The only assay in which *n-syb* mutants behaved differently from *v100* is the hypertonic stimulation (Rosenmund and Stevens, 1996). Vesicle release induced with hypertonic solution in *Drosophila* SNARE mutants is largely abolished (Aravamudan et al., 1999). In contrast, *v100* mutants exhibit some responses with a reduced number of events but normal amplitude. This implies (1) the presence of neurotransmitter-loaded vesicles in mutant terminals and (2) that SNARE function required for hypertonic release is at least partially possible. V100 is not crucial for this step, placing its role downstream of SNARE-dependent priming, congruous with the findings in yeast vacuolar fusion (Bayer et al., 2003; Peters et al., 2001; Thorngren et al., 2004). A function downstream of priming is also supported by the observation that Syx overexpression phenotypes are suppressed by the loss of *v100*.

Our results only show a late exocytic role for the  $V_0$  subunit a1, while the implication of other  $V_0$  components remains to be tested. Hence, our data is formally consistent with a role of the  $V_0$  subunit a1 outside of the  $V_0$  complex in association with SNAREs. However, to our knowledge, no role outside the  $V_0$  complex has so far been shown for a subunit a in any system. In summary, our data indicate a function for V100 and possibly the  $V_0$  proteolipid pore as a mediator of vesicle release efficiency downstream of SNARE-dependent priming.

#### Experimental Procedures

##### *Drosophila* Strains, Mutagenesis, and Screen

*y w*;  $P[\text{ry}^{+17.2} = \text{neo FRT}] 82B^{\text{isogenized}}$  flies were used for mutagenesis and unmutagenized flies used as control animals. All further fly strains are described in detail below. Mutagenesis, electroretinograms, and phototaxis assays were performed as described (Verstreken et al., 2003). The *eyFLP* screen of chromosome arm 3R is described in Mehta et al. (2005).

##### Molecular Biology and Antibody Production

###### *UAS-v100 Transgene*

LD21248 containing a full-length cDNA of CG1709 in pOT2 was obtained from the *Drosophila* Gene Collection (BDGP), and the insert was subcloned into the pUAST vector (Brand and Perrimon, 1993) at EcoRI and XhoI. Two independent insertions were recovered for each chromosome (X, 2 and 3).

###### *Antibody Production*

For details see the Supplemental Experimental Procedures. Antiserum from guinea pig 11 was used at 1:2000 on tissue and 1:10,000 on Western blots.

##### Transmission Electron Microscopy, Immunohistochemistry, Image Acquisition, and Processing

See the Supplemental Experimental Procedures.

##### Yeast Strains, Plasmids, and Methods

See the Supplemental Experimental Procedures.

##### Protein Interaction

###### *GST Pull-Downs*

Biochemical interactions of core complex proteins with  $V_0$  were determined by overnight incubation (4°C) of recombinant 0.25  $\mu\text{M}$  glutathione S-transferase (GST)-tagged proteins (GST-Syx or GST-

V<sub>0</sub>, immobilized on glutathione-Sepharose beads) with 1.0 μM purified recombinant Syx, n-Syb, or SNAP-25 in buffer A (50 mM HEPES [pH 7.4], 150 mM potassium acetate, 0.05% Tween 20). Samples were washed three times with buffer A + 1 mg/ml gelatin and two times with buffer A + 5% glycerol. Proteins were eluted in 1× sample buffer (50 mM Tris [pH 6.8], 2.5% 2-mercaptoethanol, 2% SDS, 5% glycerol).

#### Immunoprecipitations

Immunoprecipitations of core complex proteins with anti-Syx mAb 8C3 or IgG purified guinea pig anti-V<sub>0</sub> were performed using the Seize primary immunoprecipitation kit (Pierce Biotechnology, Rockford, Illinois). Per reaction, 0.5 μM Syx, n-Syb, or SNAP-25 or 500 μg adult head extract was incubated with approximately 40 μg fixed antibody in IP buffer (25 mM Tris [pH 7.2], 150 mM NaCl, 0.05% Tween 20). Samples were washed three times with IP buffer + 1 mg/ml gelatin and three times with IP buffer + 5% glycerol. Proteins were eluted in the kit's provided elution buffer. Head extract was prepared from Canton S flies using solubilization with 1% Triton X-100 for 1 hr and subsequent ultracentrifugation at 100,000 × g for 20 min to ensure the removal of membranous fragments. The preparation of head extract is described in detail in the [Supplemental Experimental Procedures](#).

#### Western Blots

See the [Supplemental Experimental Procedures](#).

#### Electrophysiology

All experiments were performed on late-stage embryos within 2–4 hr before hatching. The embryos were selected under halocarbon oil (95, Halocarbon Products, River Edge, New Jersey) for the absence of a GFP-marked balancer chromosome, and the chorion and the vitelline membrane were removed manually using sharp forceps. The embryo dissection was modified from [Broadie et al. \(1995\)](#) and was carried out in calcium-free HL3 saline: 70 mM NaCl, 5 mM KCl, 11 mM MgCl<sub>2</sub>, 10 mM NaHCO<sub>3</sub>, 5 mM trehalose, 115 mM sucrose, 5 mM HEPES. Briefly, the embryo was attached anteriorly and posteriorly to a Sylgard-coated coverslip using cyanoacrylate glue (Histoacryl B|Braun, Aesculap AG, Tuttlingen, Germany). The animal was cut open with a dorsal incision using a broken razor blade; the cut edges were attached to the coverslip with more glue, and the gut was removed to give a flat preparation with access to the body wall muscles and the nerves supplying them. The muscles were then treated with 100 U/ml of Collagenase Type 1A (Sigma-Aldrich, St. Louis, Missouri) for two minutes to remove the overlying sheath.

Whole-cell patch clamp recordings were made using an Axopatch 200B amplifier from muscle 6 of abdominal segments A2–A4 using thin-walled borosilicate pipettes fire-polished to a resistance of 3–5 MΩ. Series resistance compensation was not used. The patch pipette was filled with a solution of the following composition: 120 mM KCl, 20 mM KOH, 4 mM MgCl<sub>2</sub>, 0.25 mM CaCl<sub>2</sub>, 5 mM EGTA, 24 mM sucrose, 5 mM HEPES, and 4 mM Na<sub>2</sub>ATP. The muscle cells were clamped to –60 mV taking into account the calculated liquid junction potential of 6.7 mV. Conditions for the recording of spontaneous EPSCs, evoked EPSCs, and hypertonic stimulation are available in the [Supplemental Experimental Procedures](#).

#### FM Uptake

In brief, embryo fillets were exposed to 10 μM FM1-43FX with or without 30 mM K<sup>+</sup> for a 5 min stimulation period (stimulated and unstimulated control). The samples were subsequently extensively washed with 0 Ca<sup>2+</sup> saline for another 5 min using 0.5 mM EGTA and 1 mM Advasep-7 (Biotium, Hayward, California). Samples were then fixed and stained for another 5 min with concentrated HRP antibody (1:10) in the absence of detergent. HRP recognizes a common epitope of several neuron-specific surface molecules and thus allows us to demarcate the boundaries of the neuronal processes at the NMJ using threshold segmentation ([Figure S4B](#)). Co-labeling of HRP was similarly performed with highly concentrated Cy5-conjugated secondary antibody. Standardized 3D confocal high-resolution datasets were obtained immediately afterwards. The surface of HRP-demarcated boutons was subsequently reconstructed and the average voxel intensity in the FM1-43 channel

calculated for the total volumes inside (boutons) and outside (muscle). Finally, inside/outside ratios were calculated and are presented in [Figure 7J](#).

#### Supplemental Data

Supplemental Data include five figures and Supplemental Experimental Procedures and can be found with this article online at <http://www.cell.com/cgi/content/full/121/4/607/DC1/>.

#### Acknowledgments

We would like to thank Alois Hofbauer, Sean Carroll, Morris Manolson, Larry Zipursky, Peter Bryant, and the Bloomington Stock Center and the University of Iowa Developmental Studies Hybridoma Bank for reagents. We especially thank Iris Salecker for providing the ey3.5FLP flies prior to publication. We are indebted to Tim Fergestad and Kendal Broadie for helping with embryonic FM uptake protocols as well as Tom Lloyd for help with the Syntaxin suppressor screen. Scanning EM was performed at the High Resolution Microscopy Facility of the University of Texas MD Anderson Cancer Center with the help of Kenneth Dunner, Jr. We thank Christian Rosenmund and Erwin Neher for discussions and critical reading of the manuscript. P.R.H., A.F., R.G.Z., K.L.S., and H.J.B. are supported by the HHMI. P.R.H. was further supported by an EMBO long-term fellowship. This work was also supported by grants GM068098 from the National Institutes of Health and Q-1536 from the Welch Foundation (both to J.K.). H.J.B. is an HHMI Investigator.

Received: December 22, 2004

Revised: February 14, 2005

Accepted: March 16, 2005

Published: May 19, 2005

#### References

- Amara, S.G., and Kuhar, M.J. (1993). Neurotransmitter transporters: recent progress. *Annu. Rev. Neurosci.* 16, 73–93.
- Aravamudan, B., Fergestad, T., Davis, W.S., Rodesch, C.K., and Broadie, K. (1999). *Drosophila* UNC-13 is essential for synaptic transmission. *Nat. Neurosci.* 2, 965–971.
- Bayer, M.J., Reese, C., Bühler, S., Peters, C., and Mayer, A. (2003). Vacuole membrane fusion: V<sub>0</sub> functions after trans-SNARE pairing and is coupled to the Ca<sup>2+</sup>-releasing channel. *J. Cell Biol.* 162, 211–222.
- Bennett, M.K., Calakos, N., Kreiner, T., and Scheller, R.H. (1992). Synaptic vesicle membrane proteins interact to form a multimeric complex. *J. Cell Biol.* 116, 761–775.
- Benzer, S. (1967). Behavioral mutants of *Drosophila* isolated by countercurrent distribution. *Proc. Natl. Acad. Sci. USA* 58, 1112–1119.
- Brand, A.H., and Perrimon, N. (1993). Targeted gene expression as a means of altering cell fates and generating dominant phenotypes. *Development* 118, 401–415.
- Broadie, K., Prokop, A., Bellen, H.J., O'Kane, C.J., Schulze, K.L., and Sweeney, S.T. (1995). Syntaxin and synaptobrevin function downstream of vesicle docking in *Drosophila*. *Neuron* 15, 663–673.
- Chen, Y.A., and Scheller, R.H. (2001). SNARE-mediated membrane fusion. *Nat. Rev. Mol. Cell Biol.* 2, 98–106.
- Chou, T.B., and Perrimon, N. (1992). Use of a yeast site-specific recombinase to produce female germline chimeras in *Drosophila*. *Genetics* 131, 643–653.
- Cousin, M.A., and Nicholls, D.G. (1997). Synaptic vesicle recycling in cultured cerebellar granule cells: role of vesicular acidification and refilling. *J. Neurochem.* 69, 1927–1935.
- Deitcher, D.L., Ueda, A., Stewart, B.A., Burgess, R.W., Kidokoro, Y., and Schwarz, T.L. (1998). Distinct requirements for evoked and spontaneous release of neurotransmitter are revealed by mutations in the *Drosophila* gene *neuronal-synaptobrevin*. *J. Neurosci.* 18, 2028–2039.

- Dröse, S., and Altendorf, K. (1997). Bafilomycins and concanamycins as inhibitors of V-ATPases and P-ATPases. *J. Exp. Biol.* **200**, 1–8.
- Falk-Vairant, J., Corrèges, P., Eder-Colli, L., Salem, N., Roulet, E., Bloc, A., Meunier, F., Lesbats, B., Loctin, F., Synguelakis, M., et al. (1996). Quantal acetylcholine release induced by mediato-phore transfection. *Proc. Natl. Acad. Sci. USA* **93**, 5203–5207.
- Galli, T., McPherson, P.S., and De Camilli, P. (1996). The  $V_0$  sector of the V-ATPase, synaptobrevin, and synaptophysin are associated on synaptic vesicles in a Triton X-100-resistant, freeze-thawing sensitive, complex. *J. Biol. Chem.* **271**, 2193–2198.
- Hiesinger, P.R., Reiter, C., Schau, H., and Fischbach, K.F. (1999). Neuropil pattern formation and regulation of cell adhesion molecules in *Drosophila* optic lobe development depend on synaptobrevin. *J. Neurosci.* **19**, 7548–7556.
- Hu, C., Ahmed, M., Melia, T.J., Söllner, T.H., Mayer, T., and Rothman, J.E. (2003). Fusion of cells by flipped SNAREs. *Science* **300**, 1745–1749.
- Israël, M., Morel, N., Lesbats, B., Birman, S., and Manaranche, R. (1986). Purification of a presynaptic membrane protein that mediates a calcium-dependent translocation of acetylcholine. *Proc. Natl. Acad. Sci. USA* **83**, 9226–9230.
- Jahn, R. (2004). Principles of exocytosis and membrane fusion. *Ann. N Y Acad. Sci.* **1014**, 170–178.
- Jahn, R., Lang, T., and Südhof, T.C. (2003). Membrane fusion. *Cell* **112**, 519–533.
- Jena, B.P. (2004). Discovery of the Porosome: revealing the molecular mechanism of secretion and membrane fusion in cells. *J. Cell. Mol. Med.* **8**, 1–21.
- Kawasaki-Nishi, S., Nishi, T., and Forgac, M. (2001). Yeast V-ATPase complexes containing different isoforms of the 100-kDa a-subunit differ in coupling efficiency and *in vivo* dissociation. *J. Biol. Chem.* **276**, 17941–17948.
- Kuromi, H., and Kidokoro, Y. (2000). Tetanic stimulation recruits vesicles from reserve pool via a cAMP-mediated process in *Drosophila* synapses. *Neuron* **27**, 133–143.
- Lindau, M., and Almers, W. (1995). Structure and function of fusion pores in exocytosis and ectoplasmic membrane fusion. *Curr. Opin. Cell Biol.* **7**, 509–517.
- Mayer, A. (2002). Membrane fusion in eukaryotic cells. *Annu. Rev. Cell Dev. Biol.* **18**, 289–314.
- Mehta, S.Q., Hiesinger, P.R., Beronja, S., Zhai, R.G., Schulze, K.L., Verstreken, P., Cao, Y., Zhou, Y., Tepass, U., Crair, M.C., and Bellen, H.J. (2005). Mutations in *Drosophila sec15* reveal a specific function in neuronal targeting for a subset of exocyst components. *Neuron* **46**, 219–232.
- Meinertzhagen, I.A., and Hanson, T.E. (1993). The development of the optic lobe. In *The Development of Drosophila melanogaster*, M. Bate and A. Martinez Arias, eds. (Plainview, NY: Cold Spring Harbor Laboratory Press), pp. 1363–1491.
- Miesenböck, G., De Angelis, D.A., and Rothman, J.E. (1998). Visualizing secretion and synaptic transmission with pH-sensitive green fluorescent proteins. *Nature* **394**, 192–195.
- Morel, N. (2003). Neurotransmitter release: the dark side of the vacuolar-H<sup>+</sup>ATPase. *Biol. Cell.* **95**, 453–457.
- Morel, N., Dedieu, J.C., and Philippe, J.M. (2003). Specific sorting of the  $\alpha 1$  isoform of the V-H-ATPase a subunit to nerve terminals where it associates with both synaptic vesicles and the presynaptic plasma membrane. *J. Cell Sci.* **116**, 4751–4762.
- Nelson, N. (2003). A journey from mammals to yeast with vacuolar H<sup>+</sup>-ATPase (V-ATPase). *J. Bioenerg. Biomembr.* **35**, 281–289.
- Newsome, T.P., Åsling, B., and Dickson, B.J. (2000). Analysis of *Drosophila* photoreceptor axon guidance in eye-specific mosaics. *Development* **127**, 851–860.
- Nishi, T., and Forgac, M. (2002). The vacuolar (H<sup>+</sup>)-ATPases—nature's most versatile proton pumps. *Nat. Rev. Mol. Cell Biol.* **3**, 94–103.
- Oka, T., Toyomura, T., Honjo, K., Wada, Y., and Futai, M. (2001). Four subunit a isoforms of *Caenorhabditis elegans* vacuolar H<sup>+</sup>-ATPase. Cell-specific expression during development. *J. Biol. Chem.* **276**, 33079–33085.
- Pak, W.L., Grossfield, J., and White, N.V. (1969). Nonphototactic mutants in a study of vision of *Drosophila*. *Nature* **222**, 351–354.
- Perzov, N., Padler-Karavani, V., Nelson, H., and Nelson, N. (2002). Characterization of yeast V-ATPase mutants lacking Vph1p or Stv1p and the effect on endocytosis. *J. Exp. Biol.* **205**, 1209–1219.
- Peters, C., Bayer, M.J., Bühler, S., Andersen, J.S., Mann, M., and Mayer, A. (2001). *Trans*-complex formation by proteolipid channels in the terminal phase of membrane fusion. *Nature* **409**, 581–588.
- Pujol, N., Bonnerot, C., Ewbank, J.J., Kohara, Y., and Thierry-Mieg, D. (2001). The *Caenorhabditis elegans unc-32* gene encodes alternative forms of a vacuolar ATPase a subunit. *J. Biol. Chem.* **276**, 11913–11921.
- Richmond, J.E., and Broadie, K.S. (2002). The synaptic vesicle cycle: exocytosis and endocytosis in *Drosophila* and *C. elegans*. *Curr. Opin. Neurobiol.* **12**, 499–507.
- Rosenmund, C., and Stevens, C.F. (1996). Definition of the readily releasable pool of vesicles at hippocampal synapses. *Neuron* **16**, 1197–1207.
- Schulze, K.L., Broadie, K., Perin, M.S., and Bellen, H.J. (1995). Genetic and electrophysiological studies of *Drosophila syntaxin-1A* demonstrate its role in nonneuronal secretion and neurotransmission. *Cell* **80**, 311–320.
- Sørensen, J.B. (2004). Formation, stabilisation and fusion of the readily releasable pool of secretory vesicles. *Pflugers Arch.* **448**, 347–362.
- Stowers, R.S., and Schwarz, T.L. (1999). A genetic method for generating *Drosophila* eyes composed exclusively of mitotic clones of a single genotype. *Genetics* **152**, 1631–1639.
- Südhof, T.C. (2004). The synaptic vesicle cycle. *Annu. Rev. Neurosci.* **27**, 509–547.
- Thorngren, N., Collins, K.M., Fratti, R.A., Wickner, W., and Merz, A.J. (2004). A soluble SNARE drives rapid docking, bypassing ATP and Sec17/18p for vacuole fusion. *EMBO J.* **23**, 2765–2776.
- Verstreken, P., Koh, T.W., Schulze, K.L., Zhai, R.G., Hiesinger, P.R., Zhou, Y., Mehta, S.Q., Cao, Y., Roos, J., and Bellen, H.J. (2003). Synaptotagmin is recruited by endophilin to promote synaptic vesicle uncoating. *Neuron* **40**, 733–748.
- Weber, T., Zelman, B.V., McNew, J.A., Westermann, B., Gmachl, M., Parlati, F., Söllner, T.H., and Rothman, J.E. (1998). SNAREpins: minimal machinery for membrane fusion. *Cell* **92**, 759–772.
- Weimer, R.M., and Jorgensen, E.M. (2003). Controversies in synaptic vesicle exocytosis. *J. Cell Sci.* **116**, 3661–3666.
- Wucherpennig, T., Wilsch-Bräuninger, M., and González-Gaitán, M. (2003). Role of *Drosophila* Rab5 during endosomal trafficking at the synapse and evoked neurotransmitter release. *J. Cell Biol.* **161**, 609–624.
- Zhai, R.G., Hiesinger, P.R., Koh, T.W., Verstreken, P., Schulze, K.L., Cao, Y., Jafar-Nejad, H., Norga, K.K., Pan, H., Bayat, V., et al. (2003). Mapping *Drosophila* mutations with molecularly defined P element insertions. *Proc. Natl. Acad. Sci. USA* **100**, 10860–10865.
- Zhou, Q., Petersen, C.C., and Nicoll, R.A. (2000). Effects of reduced vesicular filling on synaptic transmission in rat hippocampal neurones. *J. Physiol.* **525**, 195–206.